Kinetic And Potential Sputtering Of Lunar Regolith: The Contribution Of The Heavy (Minority) Solar Wind Ions

F.W. Meyer[a1], P.R. Harris[a2], H.M. Meyer III[b], H. Hijazi[a], A.F. Barghouty[c]

[a]*Physics Division, Oak Ridge National Laboratory, P.O. Box 2008, Oak Ridge, TN 37831-6372, USA*
[b]*MSTD Division, Oak Ridge National Laboratory, P.O. Box 2008, Oak Ridge, TN 37831, USA*
[c]*NASA-Marshall Space Flight Center, Huntsville, AL 35812, USA*

Abstract. In this paper the sputtering of lunar regolith by protons and solar wind heavy ions is considered. From preliminary measurements of H^+, Ar^{+1}, Ar^{+6} and Ar^{+9} ion sputtering of JSC-1A AGGL lunar regolith simulant at solar wind velocities, and TRIM simulations of kinetic sputtering yields, the relative contributions of kinetic and potential sputtering contributions are estimated. An 80-fold enhancement of oxygen sputtering by Ar^+ over same-velocity H^+, and an additional x2 increase for Ar^{+9} over same-velocity Ar^+ was measured. This enhancement persisted to the maximum fluences investigated (~10^{16}/cm^2). Modeling studies including the enhanced oxygen ejection by potential sputtering due to the minority heavy ion multicharged ion solar wind component, and the kinetic sputtering contribution of all solar wind constituents, as determined from TRIM sputtering simulations, indicate an overall 35% reduction of near-surface oxygen abundance. XPS analyses of simulant samples exposed to singly and multicharged Ar ions show the characteristic signature of reduced (metallic) Fe, consistent with the preferential ejection of oxygen atoms that can occur in potential sputtering of some metal oxides.

Keywords: Solar wind, Sputtering, Lunar regolith, Ion-surface interactions.
PACS: 96.20.-n, 96.20.Ka, 68.47.Gh, 34.35.+a

INTRODUCTION

In this paper the sputtering of lunar regolith by protons and solar wind heavy ions is considered. On the basis of preliminary measurements of H^+, Ar^{+1}, Ar^{+6} and Ar^{+9} ion sputtering of JSC-1A lunar regolith simulant at solar wind velocities, performed at the ORNL Multicharged Ion Research Facility using quadrupole mass spectrometry [1], together with TRIM [2] simulations of kinetic sputtering yields, the relative contributions of kinetic and potential sputtering contributions are estimated. XPS analyses of simulant samples exposed to singly and multicharged Ar ions show the characteristic signature of reduced Fe, consistent with the preferential ejection of oxygen atoms expected in metal oxide potential sputtering.

KINETIC AND POTENTIAL SPUTTERING

Due to their low mass compared to the constituents of lunar regolith, the kinetic sputtering yields for solar wind velocity protons - the dominant solar wind constituent - are small (significantly less than unity). The minority constituents of the solar wind have significantly higher kinetic sputtering yields at solar wind velocities because of the larger mass [3] which are further enhanced by potential sputtering processes [4], since they are all multiply charged.

Kinetic sputtering originates from the collision cascade initiated by the incident ion, in which the incoming ion transfers its kinetic energy to near-surface atoms via a series of elastic binary collision encounters. Surface atoms that acquire kinetic energy higher than the surface binding energy (typically only few eV's) will be ejected.

In insulators (i.e. materials with low electron mobility) with strong electron-phonon coupling, approaching highly charged ions (HCI) can cause potential sputtering, initiated by rapid electron removal and/or particle-hole excitations in the valence band that lead to formation of localized defects such as self-trapped excitons. Such a defect decays into a non-thermal neutralized lattice anion that escapes from the surface, and a free electron, which may recombine with a surface cation to form a weakly bound neutral that may thermally desorb or be kinetically ejected. Such defect-mediated desorption [4] bears some similarity to the processes of electron- and photon-stimulated desorption.

Since lunar regolith consists mainly of metal ox-

[1] Corresponding author e-mail: meyerfw@ornl.gov
[2] Present address: United Technologies Research Center, East Hartford, CT 06108

ides [5] which are insulators, we are currently assessing the role of potential sputtering as a possible lunar surface process. Potential sputtering is strongly species selective [4], and therefore may cause significant modification of the lunar soil near-surface chemical composition and, by extension, that of the lunar exosphere, in addition to affecting overall sputtering equilibration times. As discussed in Ref. [3], knowledge of the latter is essential for comparison with other space-weathering processes such as micrometeorite impact.

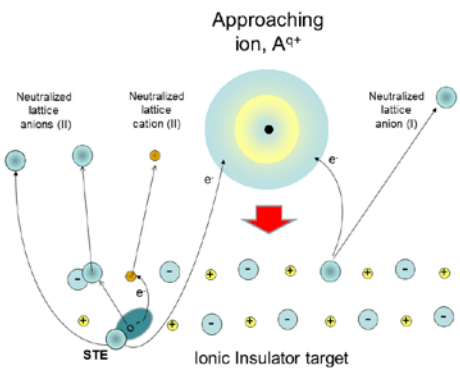

FIGURE 1. Schematic diagram of potential sputtering induced by a multicharged ion. Channel I represents resonance neutralization and can result in the ejection of a neutralized, non-thermal lattice anion (i.e. O atom in the case of a metal oxide). Channel II represents Auger neutralization that leads to production of a self-trapped exciton (STE) that decays into an F-center and H-center in the case of alkali halide targets, or E' centers in the case of SiO_2. After diffusion to the surface, the H-center desorbs as a neutralized non-thermal lattice anion while the F-center (electron) recombines with a surface cation forming a loosely bound neutral that is can be thermally desorbed or kinetically sputtered.

X-ray photoelectron spectroscopy (XPS) and Auger electron spectroscopy (AES) analyses have revealed significant near-surface metal oxide reduction (i.e. metallization) in lunar soil samples [6,7,8], particularly for Fe, but also, to reduced degrees, for Ti, Si, and Al, i.e. in inverse order of their metal-oxygen bond strength. Reduced Fe is an important determinant of lunar surface albedo, and is used (via the I_s/FeO ratio [9]) as an indicator of lunar surface maturity. The depth profile of reduced Fe is consistent with production by solar wind ion production [7].

The possibility that potential sputtering and or kinetic sputtering by the minority solar wind constituents may significantly affect the reduced Fe level in lunar soil, therefore merits further investigation. Observation of a charge state dependent enhancement of Fe reduction could also provide supportive evidence for our observed O sputtering enhancement.

OXYGEN SPUTTERING

Measurements of kinetic and potential sputtering by protons and multicharged Ar ions were carried at the MIRF using pre-sifted JSC-1A AGGL simulant pressed onto Carbon-tape (as discussed in greater detail in Ref. [1]) to compare mass-resolved sputtering in the range 2-20 amu by 375 eV/amu protons and same velocity Ar^{+}, Ar^{6+}, and Ar^{9+} ions. The Ar^{6+}, and Ar^{9+} ions were used as proxies for solar wind multicharged ions having neutralization energies in the range 300-1000 eV. To simulate the effect of the H loading of the surface due to the dominant H constituent of the solar wind, prior to each of the Ar beam exposures, the sample was exposed to a high fluence (~$10^{18}/cm^2$) of 375 eV protons. Normalized mass spectra for all three investigated species are shown in Figure 2. From the figure, a factor 80 enhancement of oxygen kinetic sputtering by Ar^{+} over same velocity protons, and an additional factor of two increase for Ar^{9+} over same velocity Ar^{+} are evident, giving a clear indication of the higher efficacy of kinetic sputtering by the heavier solar wind constituents and, further, of the importance of potential sputtering by multicharged ions.

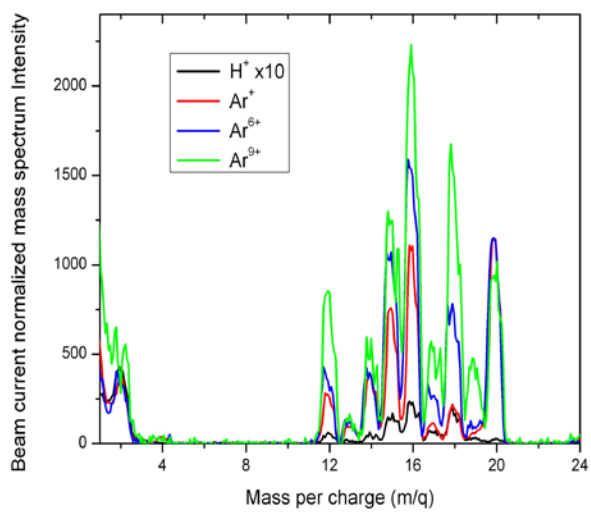

FIGURE 2. Mass distribution of sputtered species and beam species reemission in the range 2 – 24 amu, normalized to the respective beam particle currents incident on room temperature lunar regolith simulant at 375 eV/amu [1].

XPS RESULTS

In addition to the preliminary mass spectrometry-based sputtering investigations, XPS measurements of

beam-induced surface-chemistry modification were carried out, to determine if the significant O sputtering

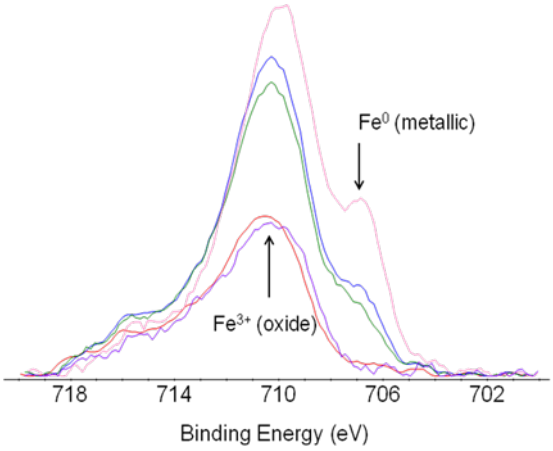

FIGURE 3. Background-subtracted Fe $2p_{3/2}$ XPS spectra for beam exposed (upper three traces) and unexposed (lower two traces) target spots. The beam exposed spots show reduced (i.e. metallic) forms of Fe. The unexposed regions show Fe in the oxidized 3+ state.

observed in the QMS measurements was correlated with changes in chemical states of metallic species in the various oxides present in the simulant. Strong evidence of Fe reduction was found in those target areas that had been exposed to high fluence Ar^{+} and Ar^{8+} beams, as illustrated in Figure 3 which shows photoelectron spectra in the Fe $2p_{3/2}$ region. Using the scanning feature of the XPS system, target maps of reduced Fe were constructed, as shown in Figure 4 (a). Preferential oxidation of the beam-exposed regions during transfer to the XPS system resulted in enhanced O concentrations in the beam-exposure regions, as seen in Figure 4 (b). An incorrect position calibration of a new manipulator resulted in some beams initially hitting the sample edge. This problem has now been fixed. The accumulated fluences for the singly and multicharged Ar beam exposures were poorly characterized in these preliminary measurements. An assessment of possible charge state enhancement effects in the Fe reduction was therefore not possible.

DISCUSSION

First, we comment on the absence of an observed dose dependence in the enhanced oxygen sputtering noted earlier. As already discussed, in the case of defect mediated sputtering of some metal oxides,

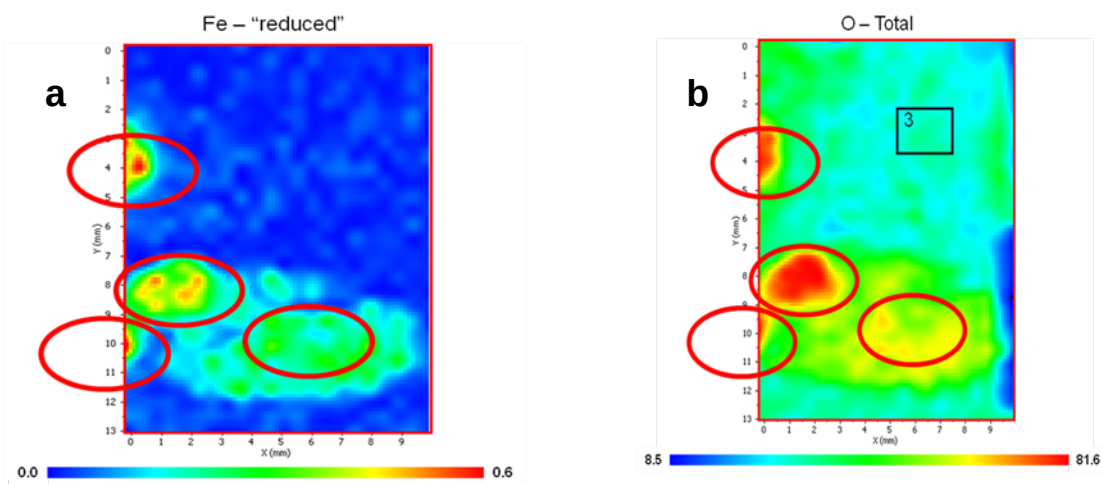

FIGURE 4. (a) Spatial intensity distribution of reduced Fe on lunar simulant sample, characterized by XPS lineshape labeled "Fe^{0} (metallic)" in Fig. 3: reduced Fe is highest in the red circles that were exposed to Ar ion beams; color scale ranges from 0 to 0.6% Fe^{0} abundance; (b) Spatial O intensity distribution on lunar simulant sample: after removing the sample from vacuum, the regions high in reduced Fe acquired additional oxygen due to preferential re-oxidation of the beam-exposed areas (red circles); color scale ranges from 8.5 to 81.6% O abundance; area "3" - background area where lower two XPS scans in Figure 3 were measured.

preferential (or nonstoichiometric) sputtering of the anion component (in this case oxygen atoms) of the metal oxide will occur if the neutralized cation (metallic) products, also arising from this process, are not thermally desorbed, or are not ejected by momentum transfer from the incident projectiles. In this case, surface metallization will gradually occur, and the surface requirements for potential sputtering are eventually no longer satisfied. As a consequence, the yield enhancement due to potential sputtering will disappear beyond a certain incident ion fluence, as has been observed at very low impact energies [10]. Wurz

et al. [11] used this observation to argue that potential sputtering is negligible in solar wind sputtering. This argument is not believed to be valid, since solar wind ion impact energies exceed the physical sputtering threshold energies of virtually all species present in lunar regolith. At solar wind energies, the more weakly bound neutralized surface cations also arising in the process are therefore physically sputtered as well, and surface metallization is impeded.

This conclusion is supported by Figure 5, which shows the combined effect of physical and potential sputtering on the composition of a KREEP model lunar surface [see Ref. 3 for details]. The sputtering-induced surface-compositional changes are simulated using a dynamical elemental surface composition model that incorporates all solar wind constituents, the TRIM-based kinetic sputtering yields of all KREEP constituents and, in addition, potential sputtering yields of oxygen. The O potential sputtering yields are based on our preliminary experimental sputtering re-

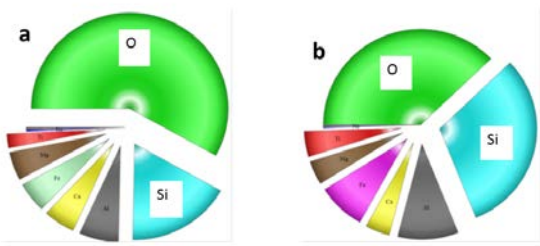

FIGURE 5. (a) Comparison of KREEP bulk model lunar regolith composition, and (b) a KREEP surface exposed to kinetic and potential solar wind sputtering after reaching steady state; note the O abundance in (b) is reduced by ~35% (for more details, see Ref. [3]). The remaining KREEP elemental constituents shown in the figure are, clockwise after Si: Al, Ca, Fe, Mg, Ti, and Na.

sults, and extended to the other multicharged heavy ion constituents of the solar wind as described in Ref. [3]. As illustrated in the figure, for the KREEP surface, the elemental oxygen abundance is reduced by the solar wind impact, with roughly equal contributions from kinetic and potential sputtering. Accompanying the ~35% O reduction are, of course, corresponding increases in the metal species abundances, but not to the limit of a highly metallized surface, as assumed by Wurz et al. [11]. It is important to recall that this analysis does not yet include potential sputtering of KREEP elemental constituents other than oxygen. Comparison with the observed stoichiometry of grains from Apollo lunar samples [e.g. 14] is therefore premature.

As discussed in greater detail in Ref. [3], another effect of the enhanced sputtering by heavy solar wind ions is a ~38% reduction in the characteristic sputtering time scale to reach a steady state surface composition. This consequence is important since it affects comparison with the competing time scale of surface "gardening" by micrometeorite impacts [12,13] which exposes a fresh bulk surface for modification by solar wind sputtering.

ACKNOWLEDGMENTS

Research sponsored by the Laboratory Directed Research and Development Program of Oak Ridge National Laboratory, managed by UT-Battelle, LLC, for the U. S. Department of Energy, by NASA grant 10-LASER10-0053, and by the Division of Chemical Sciences, Geosciences, and Biosciences, Office of Basic Energy Sciences, of the USDOE.

REFERENCES

1. Meyer, F.W., Harris, P.R., Taylor, C.N., Meyer III, H.M., Barghouty, A.F., Adams, J.H., *Nucl. Inst. and Meth. B* ***269***, 1316-1320 (2011).
2. Ziegler, J.F., Biersack, J.P., Littmark, U., *The Stopping and Range of Ions in Solids*, edited by R. B. Hamil, New York: Pergamon, 1996.
3. Barghouty, A.F., Meyer; F.W., Harris; P.R., Adams,J.H., *Nucl. Inst. and Meth. B* **269**, 1310-1315 (2011).
4. Aumayr, F., and Winter, H.P., *Phil. Trans. R. Soc. Lond. A* **362**, 77-102 (2004).
5. Heiken, G.H., Vaniman, D.T., and French, B.M., Chapter 7 in *Lunar Source Book: A User's Guide to the Moon*, Cambridge: Cambridge Univ. Press, 1991. CD version by Lunar and Planetary Institute, 3600 Bay Area Boulevard, Houston, TX 77058-1113 (2005).
6. Dikov, Yu.P., Bogatikov, O.A., Barsukov, V.L., Florensky, K.P., Ivanov, A.V., Nemoshkalenko, V.V., and Alyoshin, V.G., *Proc. 10th Lunar Planet. Sci. Conf.*, 1491 (1979).
7. Dikov, Yu.P., Bogatikov, O.A., Barsukov, V.L., Florensky, K.P., Ivanov, A.V., Nemoshkalenko, V.V., Alyoshin, V.G. and Chudinov, M.G., *Proc. 9th Lunar Planet. Sci. Conf*., 2111 (1978).
8. Loeffler, M.J., Dukes, C.A., and Baragiola, R.A., *J. Geophys. Res.* **114**, E03003, doi:10.1029/2008JE003249, (2009).
9. von Steiger, R., Schwadron, N.A., Fisk, L.A., Geiss, J., Gloecker, G., Hefti, S., Wilken, B., Wimmer-Schweingruber, R.F., and Zurbuchen, T.H., *J. Geophys. Res.* **105**, 217-227 (2000).
10. Hayderer, G., Cernusca, S., Hoffmann, V., Niemann, D., Stolterfoht, N., Schmid, M., Varga, P., Winter, HP., and Aumayr, F., *Nucl. Inst. and Meth. B* ***18***, 143-147 (2001).
11. Wurz, P., Rohner, U., Whitby, J.A., Kolb, C., Lammer, H., Dobniker, P., and Martin-Fernandez, J.A., *Icarus* **191**, 486-496 (2007.
12 Starukhina, L.V., *Solar Syst. Res.* **37**, 36 (2003).
13. Starukhina, L.V., Shkuratov, Y.G., *Icarus* **147**, 585 (2000).
14. Johnson, R.E. and Baragiola, R., *Geophys. Res. Lett.* **18**, 2169 (1991).